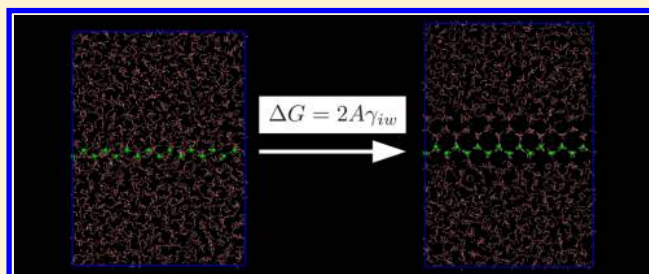


# Ice–Water Interfacial Free Energy for the TIP4P, TIP4P/2005, TIP4P/Ice, and mW Models As Obtained from the Mold Integration Technique

Jorge R. Espinosa, Carlos Vega, and Eduardo Sanz\*

Departamento de Química Física, Facultad de Ciencias Químicas, Universidad Complutense de Madrid, 28040 Madrid, Spain

**ABSTRACT:** The freezing of water is greatly influenced by the ice–water interfacial free energy. Yet, no consistent experimental measures of this thermodynamic parameter can be found. In this work we provide estimates for the ice Ih–water interfacial free energy at the normal melting temperature for different crystal planes (basal, primary prismatic, and secondary prismatic) using some widely used water models: TIP4P, TIP4P/2005, TIP4P/Ice, and mW. To compute the interfacial free energy, we use the mold integration method. It consists in calculating the work needed to induce the formation of a crystal slab in the fluid at coexistence conditions with the aid of a mold of potential energy wells whose structure is that of the crystal plane under study. The basal plane has the lowest interfacial free energy in all models of the TIP4P family. For the mW model we could not resolve differences in interfacial free energy between different orientations. The interfacial free energies averaged over all crystal orientations we obtain are 27.2(8), 28.9(8), 29.8(8), and 34.9(8) mJ/m<sup>2</sup> for the TIP4P, TIP4P/2005, TIP4P/Ice, and mW models, respectively. The averaged interfacial free energy increases with both the melting temperature and melting enthalpy of the model. Moreover, we compute the interfacial free energy for several crystal orientation of ice Ic using the TIP4P/Ice model and obtain within the accuracy of our calculations the same orientationally averaged interfacial free energy as that of ice Ih. Our results are in good agreement with previous estimates of the interfacial free energy based on a classical nucleation theory analysis of simulations of spherical ice seeds embedded in supercooled water.



## INTRODUCTION

The crystal nucleation rate and the shape and speed with which crystals grow are greatly affected by the free energy cost of forming an interface between the emerging crystal and the surrounding fluid. Therefore, obtaining accurate values of the crystal–fluid interfacial free energy is of central importance.<sup>1</sup> Yet, there are no reliable experimental techniques to measure such thermodynamic parameter. For instance, for the ice–water interface values ranging from 25 to 35 mJ/m<sup>2</sup> have been reported.<sup>2,3</sup> A precise value for the ice–water interfacial free energy,  $\gamma_{iw}$  is needed, for instance, to interpret measurements of the ice nucleation rate,<sup>2–14</sup> a property that plays an important role in atmospheric physics and climate change models.<sup>15–17</sup>

In the absence of reliable experimental values, estimates of  $\gamma_{iw}$  can be obtained from simulations of realistic water models. The first direct calculation of  $\gamma_{iw}$  was performed using an improved version of the cleaving method<sup>18,19</sup> for the TIP4P model.<sup>20</sup> In ref 21 such calculations were improved by including full electrostatic interactions, and in addition, values for the TIP4P-Ew and TIP5P-E models were also reported. By employing a method based on the analysis of capillary fluctuations,<sup>22</sup>  $\gamma_{iw}$  was recently computed for the TIP4P/2005<sup>23</sup> and mW water models.<sup>24</sup> With the exception of ref 24, all the calculations of  $\gamma_{iw}$  previously mentioned correspond to the flat ice–water interface at the normal melting temperature of the model. To the best of

our knowledge, these are the only direct calculations of  $\gamma_{iw}$ . Given that the same model has not been studied by different groups, more work is needed to reach a consensus on the value of  $\gamma_{iw}$  for the most popular water models.

With the aim of establishing definite values for  $\gamma_{iw}$  for some widely used water models, we perform direct calculations of  $\gamma_{iw}$  using the mold integration (MI) method<sup>25</sup> for the TIP4P,<sup>26</sup> TIP4P/2005,<sup>27</sup> TIP4P/Ice,<sup>28</sup> and mW<sup>29</sup> models. Our results can also be useful to validate the analysis of simulation studies of ice nucleation<sup>30–36,38–46</sup> using classical nucleation theory.<sup>47–51</sup> These studies provide estimates of  $\gamma_{iw}$  for a curved ice–water interface at temperatures below melting. The validity of such estimates can be assessed by extrapolating the results to coexistence conditions and comparing with direct calculations of  $\gamma_{iw}$ . By contrast to the estimates based on nucleation studies, where a  $\gamma_{iw}$  averaged over all crystal orientations is obtained, the method employed in this work allows for the calculation of  $\gamma_{iw}$  for specific crystal orientations. We compute  $\gamma_{iw}$  for hexagonal ice, ice Ih, and three different crystal planes exposed to the fluid: basal, primary prismatic (pI), and secondary prismatic (pII). We also evaluate  $\gamma_{iw}$  for the (111), (100), and (110) planes of ice Ic. The comparison between the interfacial free

Received: November 16, 2015

Revised: April 1, 2016

Published: April 13, 2016

energies of cubic (ice Ic) and hexagonal (ice Ih) ice can shed light on the role of these stacking polymorphs in the initial stages of ice nucleation and growth.<sup>10,32,37,40,41,52–60</sup>

## SIMULATION DETAILS

To simulate the TIP4P family models, we use molecular dynamics with the GROMACS package.<sup>61</sup> All runs are performed at constant pressure of 1 bar. Pressure is only exerted along the direction perpendicular to the interface whose growth is induced within the MI scheme. In our coordinate system this is the  $x$  direction, so all runs are performed in the  $Np_xT$  ensemble. To avoid stress, the  $L_y$  and  $L_z$  edges of the simulation box are fixed to a value consistent with the equilibrium unit cell at coexistence conditions. All simulations are run at the constant pressure of  $p = 1$  bar, using an anisotropic Parrinello–Rahman barostat<sup>62</sup> with a relaxation time of 0.5 ps. To fix the temperature, we employ a velocity-rescale thermostat<sup>63</sup> with a relaxation time of 0.5 ps. The time step for the Verlet integration of the equations of motion is 1.5 fs. We use particle mesh Ewald summations<sup>64</sup> to deal with electrostatic interactions. The cutoff radius for both dispersive interactions and the real part of electrostatic interactions is 14 Å. The interaction between the mold and the water molecules is provided to GROMACS in a tabular form (this precludes using long-tail corrections for the Lennard–Jones interaction).

To simulate the mW model, we use a bespoke Monte Carlo code. Monte Carlo runs are performed at 1 bar and in the  $Np_xT$  ensemble. The shifts for the trial displacements and volume moves are tuned during equilibration to get an acceptance rate of 35–45%. A Monte Carlo sweep consists in a trial displacement move per particle plus a trial volume move.

## MOLD INTEGRATION METHOD

The MI method for the calculation of the crystal–fluid interfacial free energy has been recently proposed by us.<sup>25</sup> There are other methods to directly compute the interfacial free energy at coexistence,<sup>18,22,65–70</sup> but MI is particularly suited for the present study because it can be combined with GROMACS and it does not require a large number of particles. The MI method was originally validated with the calculation of the interfacial free energy of the Lennard–Jones and hard spheres systems<sup>25</sup> and later on applied to sodium chloride.<sup>71</sup> We refer the reader to these publications for a detailed description of the method. In brief, the MI method consists in computing the reversible work needed to induce the formation of a crystal slab in a fluid at coexistence conditions (at the normal melting temperature in our case, reported in Table 3 for the employed water models). Such work is a Gibbs free energy difference,  $\Delta G$ , and is related to the interfacial free energy by

$$\Delta G = 2A\gamma_{\text{iw}} \quad (1)$$

where  $A$  is the area of the simulation box side in the direction perpendicular to the mold (the factor of 2 is due to the fact that two interfaces are generated). The formation of the crystal slab is induced by switching on an attractive interaction between a mold composed of potential energy wells and the fluid particles. The wells are placed in the equilibrium positions of the oxygen atoms of the ice lattice plane of interest at coexistence conditions. In Figure 1 we show a mold for the pII plane, and in Figure 2 we show how such mold is able to induce the formation of an ice slab in liquid water at coexistence conditions. If the interaction between the wells and the oxygen

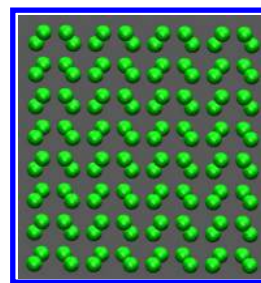


**Figure 1.**  $y$ – $z$  projection of a mold of 128 potential wells placed at the oxygen lattice positions of a pII plane at the TIP4P/Ice coexistence conditions ( $p = 1$  bar,  $T = 270$  K).

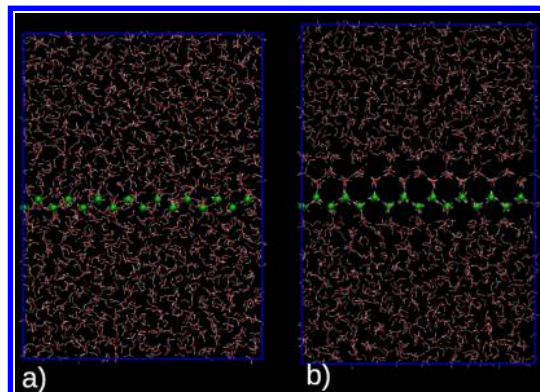


**Figure 2.** Snapshots of a TIP4P/Ice configuration at 1 bar pressure and 270 K (coexistence conditions). The mold of potential energy wells is represented by the green spheres. Its interaction with water molecules is switched off in (a) and on in (b). The radius of the mold's wells is 0.91 Å in this case.

atoms of the water model is square-well-like (with maximum well depth  $\epsilon_m$  and well radius  $r_w$ ),  $\gamma_{\text{iw}}$  can be obtained as<sup>25</sup>

$$\gamma_{\text{iw}}(r_w) = \frac{1}{2A}(\epsilon_m N_w - \int_0^{\epsilon_m} \text{d}\epsilon \langle N_{\text{fw}}(\epsilon) \rangle_{Np_xT}) \quad (2)$$

where  $N_w$  is the total number of wells and  $\langle N_{\text{fw}}(\epsilon) \rangle$  is the average number of filled wells obtained in the  $Np_xT$  ensemble for wells of depth  $\epsilon$ . Basically, one has to perform thermodynamic integration along a path in which the depth of the wells is gradually increased to its maximum value,  $\epsilon_m$ . The integration in eq 2 must be reversible. To ensure reversibility, the structure induced by the mold must quickly disappear when the interaction between the mold and the fluid is switched off. Therefore, one has to make sure that the ice slab does not fully form in the integration. This is prevented by performing thermodynamic integration for wells whose radius is wider than a certain value  $r_w^0$ . In practice,  $\gamma_{\text{iw}}(r_w)$  is estimated for several values of  $r_w > r_w^0$  and then  $\gamma_{\text{iw}}(r_w)$  is extrapolated to  $r_w^0$ , which is the well radius that gives the correct value of  $\gamma_{\text{iw}}$  (see ref 25).

To implement the well–oxygen interaction,  $v_{\text{wo}}$ , in molecular dynamics, we use a continuous version of the square-well potential:<sup>25</sup>

$$v_{\text{wo}} = -\frac{1}{2}\epsilon \left[ 1 - \tanh\left(\frac{r - r_w}{\alpha}\right) \right] \quad (3)$$

where  $r$  is the distance between the well center and the oxygen atom with which the well interacts, and  $\alpha$  is a parameter that controls the steepness of the well's walls.  $\alpha$  cannot be too large

to avoid strong forces acting on the particles trapped inside the wells. We find that  $\alpha = 0.017 \text{ \AA}$  works well for the case of water.

## RESULTS

**Determination of  $r_w^o$ .** The first step is to make sure that one is indeed able to induce an ice slab using the selected mold. This should happen for small well radii. In Figure 2 we show that using a pII mold with well radius =  $0.91 \text{ \AA}$ , an ice slab does grow from the fluid. Note that only the oxygen atoms interact with the mold. Once the mold is filled with oxygens the system is able to build up the hydrogen bond network on its own.

After having tested the ability of the molds to induce the formation of an ice slab, the next step is to find the optimal well radius,  $r_w^o$  (that for which the right  $\gamma_{iw}$  is obtained). This is done by performing several trajectories for different  $r_w$ 's, all starting from a fluid configuration. The mold is fully switched on ( $\epsilon = \epsilon_m$ ) at the beginning of each trajectory. If  $r_w \leq r_w^o$ , an ice slab should grow in all trajectories with no induction period given that there is no free energy barrier for the formation of the crystal. On the contrary, if  $r_w > r_w^o$ , a barrier must be overcome, which is reflected in some trajectories having an induction period before the slab grows or even in no slab formation at all if  $r_w$  is too large.<sup>25</sup> To know if a crystal slab grows, we monitor  $n_s$ , the number of molecules in the largest crystal cluster (to compute  $n_s$  we follow the procedure described in ref 30 that makes use of the order parameter proposed in ref 72). The trajectories used to find  $r_w^o$  for the pII mold of Figure 1 are shown in Figure 3. The situation previously described for  $r_w \leq r_w^o$  corresponds to the top panels ( $r_w = 0.919$  and  $0.953 \text{ \AA}$ ), whereas that for  $r_w > r_w^o$  corresponds to the bottom panels ( $r_w = 0.987, 1.022,$  and  $1.192 \text{ \AA}$ ). The largest  $r_w$  that does not show any run with an induction period is  $r_w = 0.953 \text{ \AA}$ , and the

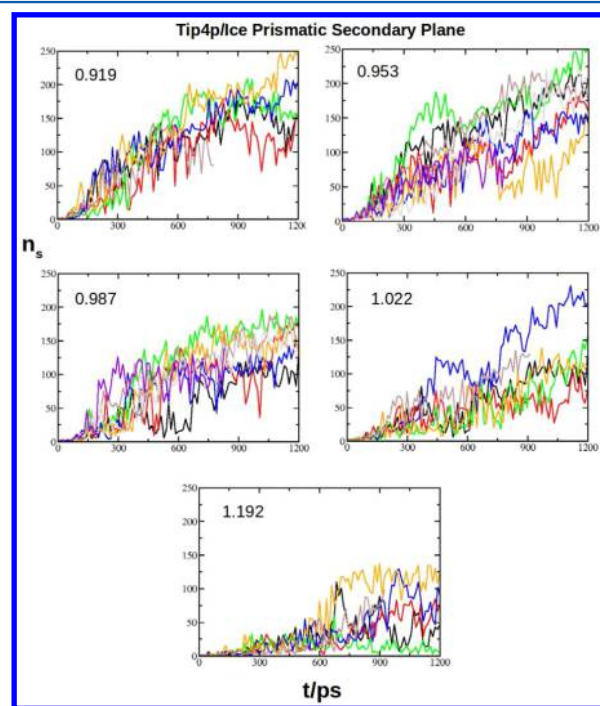


**Figure 3.** Number of particles in the largest crystal cluster,  $n_s$ , versus time for several trajectories and different well radii (as indicated in the legend in  $\text{\AA}$ ) for the pII plane of the TIP4P/Ice model. All simulations are performed at coexistence conditions (1 bar, 270 K). In all cases  $\epsilon = \epsilon_m = 8k_B T$ .

smallest one in which at least one run shows induction period is  $r_w = 0.987 \text{ \AA}$ . Therefore, we find  $r_w^o = 0.97 \pm 0.05 \text{ \AA}$ . We acknowledge that the presence of trajectories with an induction period for  $r_w = 0.987 \text{ \AA}$  may not be entirely clear in view of Figure 3. In order to be safe, the error bar we give for  $r_w^o$  includes cases where the absence/presence of trajectories with induction period is absolutely clear. The error in  $r_w^o$  is in fact the main source of uncertainty in our calculation of  $\gamma_{iw}$ .

In Table 1 we report  $r_w^o$  for all crystal planes and water models studied in this work, along with the area of the simulation box side parallel to the mold,  $L_y L_z$ , the number of wells in the mold,  $N_w$ , and the number of water molecules used in the simulation,  $N$ . Note that  $r_w^o$  depends on the model and on the crystal plane. In all cases  $r_w^o$  takes the lowest value for the pI plane and the highest value for the pII plane.

**Thermodynamic Integration.** Once  $r_w^o$  is known, we compute the integral given in eq 2 for values of  $r_w$  larger than  $r_w^o$ . As an example, the integrand of eq 2 for the pII plane of the TIP4P/Ice model is shown in Figure 4. Each point corresponds to a different depth of the square well interaction between the wells and the oxygen atoms. The integrand reaches a plateau for large values of  $\epsilon$  given that the average number of filled wells is nearly  $N_w$  beyond a certain value of the well depth. Once the plateau is reached the value of  $\gamma(r_w)$  given by eq 2 does not almost depend on  $\epsilon_m$ , which in our case is  $8k_B T$ .

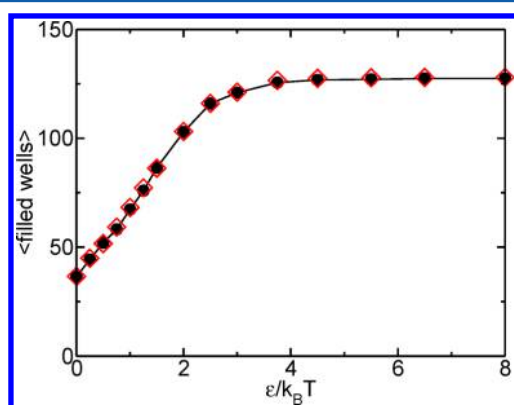
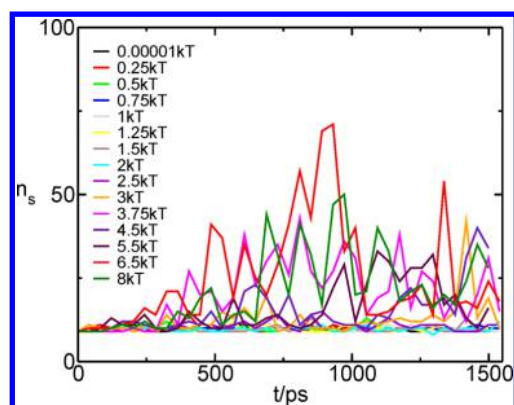
To make sure that the thermodynamic integration is reversible, it is advisable to check that  $n_s$  does not grow at any integration point. This kind of check is shown in Figure 5. For the  $r_w$  employed in this integration ( $1.3 \text{ \AA}$ ), none of the runs show a growing  $n_s$ . For the deepest wells ( $\epsilon = 6.5k_B T$  and  $8k_B T$ ) there is an incipient crystal slab forming and melting, as inferred from the large fluctuations in  $n_s$ . However, the incipient slab forms and redissolves quickly, and thermodynamic integration can be safely performed. We further check the reversibility of the thermodynamic integration by looking at the impact of the initial configuration on the calculations. All the black points in Figure 4 were obtained by using a fluid configuration as a starting point. We now use the final configuration of the simulation with the mold fully switched on ( $\epsilon = \epsilon_m = 8k_B T$ ) to repeat the calculations. If a crystal slab had been irreversibly formed, we would not obtain the same integrand. The test is satisfactory, though, and we obtain the red diamonds in Figure 4.

For every model and crystal orientation we have performed thermodynamic integration for 3–4 different values of  $r_w > r_w^o$ . The resulting values of  $\gamma_{iw}(r_w)$  are shown in Figure 6 with solid symbols.

**Interfacial Free Energy,  $\gamma_{iw}$ .** The  $\gamma_{iw}(r_w)$  points corresponding to a given model and crystal plane are fitted to a straight line to extrapolate the results to  $r_w^o$ , where we read the definite value for  $\gamma_{iw}$  (shown with empty symbols in Figure 6). Although we do not have a definite proof that the  $\gamma_{iw}(r_w)$  dependence is linear, we have several indications to believe so. On the one hand, for all water models studied in this work and for the hard sphere, Lennard-Jones, and NaCl models investigated in refs 25 and 71, we get a linear  $\gamma_{iw}(r_w)$  dependence in the  $r_w$  range where the calculations were performed. On the other hand, the linear extrapolation to  $r_w = r_w^o$  has given consistent results with direct calculations of the interfacial free energy using other methods for hard spheres, Lennard-Jones, NaCl (see refs 25 and 71), and water (see below).

**Table 1.**  $\gamma_{iw}$  for All Water Models and Crystal Orientations Studied for Ice Ih, Details on System Size and Parameters Used for the Calculation (See Main Text), and for Comparison Results from Other Works

model	crystal plane	$(L_y \times L_z)$ ( $\text{\AA}^2$ )	$N_w$	$N$	$r_w^o$ ( $\text{\AA}$ )	$\gamma_{iw}$ ( $\text{mJ/m}^2$ )	$\gamma_{iw}^{\text{lit}}$ ( $\text{mJ/m}^2$ )
TIP4P/Ice	basal (0001)	1141.2	128	1792	0.83(5)	27.2(8)	
TIP4P/Ice	pI (10 $\bar{1}$ 0)	1075.9	128	1792	0.77(5)	31.6(8)	
TIP4P/Ice	pII (11 $\bar{2}$ 0)	931.69	128	1280	0.97(5)	30.7(8)	
TIP4P/Ice	$\gamma_0$					29.8(8)	30.8(2.5) <sup>31</sup>
TIP4P/2005	basal	1128.7	128	1792	0.83(5)	27.2(8)	27(2) <sup>23</sup>
TIP4P/2005	pI	1064.1	128	1792	0.73(5)	29.5(8)	28(2) <sup>23</sup>
TIP4P/2005	pII	921.55	128	1280	0.94(5)	30.0(8)	28(2) <sup>23</sup>
TIP4P/2005	$\gamma_0$					28.9(8)	29.0(2.5) <sup>31</sup>
TIP4P	basal	1113.5	128	1792	0.83(5)	25.5(8)	24.5(6) <sup>21</sup>
TIP4P	pI	1049.8	128	1792	0.77(5)	28.2(8)	27.6(7) <sup>21</sup>
TIP4P	pII	909.09	128	1280	1.12(5)	28.0(8)	27.5(7) <sup>21</sup>
TIP4P	$\gamma_0$					27.2(8)	25.6(2.5) <sup>31</sup>
mW	basal	1084.4	128	1792	1.00(5)	34.5(8)	
mW	pI	1022.4	128	1792	0.63(5)	35.1(8)	
mW	pII	885.39	128	1280	1.00(5)	35.2(8)	
mW	$\gamma_0$					34.9(8)	35.2(2.5), <sup>73</sup> 35(2) <sup>74</sup>

**Figure 4.** Average number of filled wells versus well depth ( $\epsilon/k_B T$ ) for the pII plane of the TIP4P/Ice model. The radius of the mold wells is 1.30  $\text{\AA}$ . All simulations are performed at 1 bar and 270 K. Each point corresponds to an  $Np_x T$  simulation with 0.5 ns of equilibration and 1 ns of production (for the mW model we performed for each integration point 10 000 MC sweeps to equilibrate the system and an extra 40 000 to obtain  $\langle N_{iw} \rangle$ ). Black circles (empty diamonds) correspond to simulations starting from an equilibrated configuration with the mold switched off (on).**Figure 5.**  $n_s$  versus time for all integration points shown in Figure 4. Indicated in the legend is the well depth in  $k_B T$ .

The values of  $\gamma_{iw}$  linearly extrapolated to  $r_w^o$  for each water model and crystal orientation are reported in Table 1. For all

models of the TIP4P family the basal plane has the lowest  $\gamma_{iw}$  and both prismatic planes have the same  $\gamma_{iw}$  within the error of our calculations. For mW we also obtain a lower  $\gamma_{iw}$  for the basal plane, although the error bar overlaps with those of the prismatic planes. Our results for the TIP4P, TIP4P/2005, and mW models are consistent with those of refs 21, 23, and 74, respectively, where  $\gamma_{iw}$  was directly computed at coexistence conditions. Our work improves the calculations reported in refs 23 and 74 though. On the one hand, our results for the TIP4P/2005 model are more accurate than those of ref 23, where the anisotropy of  $\gamma_{iw}$  with the crystal orientation could not be resolved using the capillary fluctuation method. We do see now that the basal plane has lower interfacial free energy than the prismatic planes. Regarding the mW model, in ref 74 it was not specified whether  $\gamma_{iw}$  was obtained for a spherical cluster or for a planar interface, whereas in this work we report the interfacial free energy for the three main orientations of the ice Ih lattice.

It is not obvious why the basal plane has a lower interfacial free energy than the prismatic ones, although here we provide a speculative explanation based on two previous observations. On the one hand, the penalty paid by creating the ice–water interface is entropic (the interfacial enthalpy is actually negative).<sup>30,34</sup> On the other hand, it has been shown that the freedom to stack growing ice planes in two different positions confers some degree of disorder to the basal interface.<sup>23,75</sup> In particular, alternating patches of hexagonal and cubic ice have been observed in simulations of the basal interface, both at rest<sup>23</sup> and during ice growth<sup>75</sup> (in fact, the growth of the basal interface is delayed by the competition between such patches<sup>75</sup>). This mixed interfacial pattern may increase the entropy of the basal interface and thus reduce the entropic cost of forming it. Because there is only one way of stacking a growing ice layer for both prismatic planes, these cannot benefit from a disordered interfacial pattern. This kind of reasoning could also justify that the (111) plane in the hard sphere and Lennard-Jones systems has a lower interfacial free energy than the (100) one.<sup>25</sup> We are unable to explain, though, why the entropic stabilization of the basal plane is more noticeable for the TIP4P models than for mW.

We now focus the discussion on  $\langle \gamma_{iw} \rangle$ , the ice–water interfacial free energy averaged over all crystal orientations. The mW model has the highest  $\langle \gamma_{iw} \rangle$ , 34.9(8)  $\text{mJ/m}^2$ , then goes the

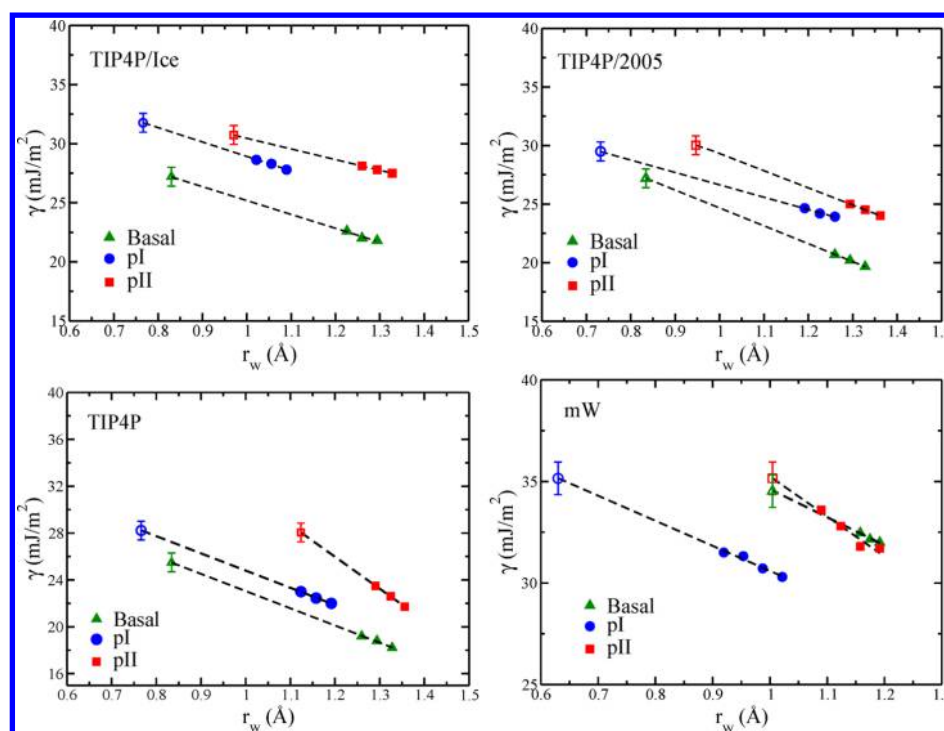


**Figure 6.** Filled symbols: interfacial free energy for different values of the well radius and crystal orientations of ice Ih, as indicated in the legend (statistical errors have the size of the symbols). Dashed lines: linear fits to filled symbols. Empty symbols: extrapolation of the linear fits to the optimal well radius.

TIP4P/Ice with 29.8(8) mJ/m<sup>2</sup>, followed by the TIP4P/2005 and TIP4P with 28.9(8) and 27.2(9) mJ/m<sup>2</sup>, respectively.

We have checked that the orientationally averaged interfacial free energy,  $\gamma_0$ , obtained from an expansion of  $\gamma_{iw}$  in spherical harmonics<sup>76</sup> (see Table 2 of ref 23) gives the arithmetic average of  $\gamma_{iw}$  for the three main crystal orientations,  $\langle \gamma_{iw} \rangle$ . Therefore, we can compare our  $\langle \gamma_{iw} \rangle$ 's with those obtained from the seeding technique (a classical nucleation theory analysis of simulations of spherical clusters embedded in the supercooled fluid<sup>30,73,77–79</sup>) for the TIP4P, TIP4P/Ice, TIP4P/2005<sup>31</sup> and mW<sup>73</sup> models. As shown in Table 1, the agreement between seeding and MI is quite good. Such consistency, alongside that reported for the hard spheres, Lennard-Jones, and NaCl systems,<sup>73</sup> supports that classical nucleation theory<sup>47–51</sup> provides a good description of crystal nucleation.

In a recent publication we reported that the seeding method gives the same  $\gamma_{iw}$  for spherical ice Ic and ice Ih seeds.<sup>32</sup> To corroborate this finding, we examine the interfacial free energy of different ice Ic planes for the TIP4P/Ice model. Details on the calculations are given in Table 2. Two of the ice Ic planes considered have the same interplanar spacing as an ice Ih counterpart: the ice Ic (110) plane corresponds to the pII ice Ih plane and the ice Ic (111) plane to the basal ice Ih plane. In fact, we obtain similar values of  $\gamma_{iw}$  for corresponding planes

**Table 2.**  $\gamma_{iw}$  for Ice Ic and Several Crystal Orientations Using the TIP4P/Ice Model, Details on System Size, and Parameters Used for the Calculation (See Main Text)

crystal plane	$(L_y \times L_z)$ (Å <sup>2</sup> )	$N_w$	$N$	$r_w^c$ (Å)	$\gamma_{iw}$ (mJ/m <sup>2</sup> )
(100)	1029.4	100	1800	0.90(5)	31.0(8)
(110)	1164.6	160	1920	0.99(5)	31.4(8)
(111)	931.69	128	1280	0.85(5)	26.9(8)

(see Tables 2 and 1). The ice Ic (111) and the ice Ih basal planes differ in the way hexagonal planes are stacked (ABC vs ABAB). Computing the impact on  $\gamma_{iw}$  of such stacking difference would require using molds with at least three hexagonal planes (we use one here to ensure reversibility in the thermodynamic integration). The effect of stacking is expected to be minor, though, as suggested both by the alternating cubic/hexagonal pattern of the basal interface<sup>23</sup> and by the stacking disorder often observed in ice growth simulations.<sup>41,60,75,80,81</sup> The (100) ice Ic plane does not have any ice Ih counterpart. Its  $\gamma_{iw}$  is similar to that of the prismatic ice Ih planes. With the values of  $\gamma_{iw}$  computed for three different orientations, and using an expansion of  $\gamma_{iw}$  in terms of cubic harmonics,<sup>82,83</sup> we obtain  $\gamma_0 = 30.1(8)$  mJ/m<sup>2</sup>, which is similar to the value of  $\gamma_0 = 29.8(8)$  mJ/m<sup>2</sup> obtained for ice Ih. This result is consistent with the observation reported in ref 32 that spherical seeds of ice Ih and ice Ic of the same size are critical at the same temperature.

We finally seek a relation between the interfacial free energy and other thermodynamic parameters of the model. Turnbull empirically observed the following relation in crystal nucleation studies:<sup>88</sup>

$$\frac{\gamma \rho^{-2/3}}{\Delta h_m} = c_T \quad (4)$$

where  $\gamma$  is the crystal–fluid interfacial free energy,  $\rho$  is the number of molecules per unit volume in the crystal (so  $\rho^{-2/3}$  is an estimate of the mean area per molecule at the interface),  $\Delta h_m$  is the melting enthalpy per molecule, and  $c_T$  is a constant that Turnbull found to be 0.45 for many metals and 0.32 for water, Bi, Sn, and Ge. Laird proposed an alternative relation by substituting  $\Delta h_m$  in Turnbull's expression by the thermal energy,  $k_B T$ , at the melting temperature,  $T_m$ .<sup>89</sup>

Table 3. Melting Properties and Turnbull's and Laird's Constants for the Models Studied in the Work<sup>a</sup>

model	$\langle\gamma_{iw}\rangle$	$T_m$ (K)	$\Delta H_m$	$\Delta S_m$	$\rho_i$ (g/cm <sup>3</sup> )	$c_T$	$c_L$
TIP4P	27.2	230 <sup>84</sup>	1.05	4.56	0.940	0.37(2)	0.86(4)
TIP4P/2005	28.9	250 <sup>80,84,85</sup>	1.16	4.64	0.921	0.37(2)	0.85(4)
TIP4P/Ice	29.8	270 <sup>86,87</sup>	1.29	4.78	0.906	0.34(2)	0.82(4)
mW	34.9	274 <sup>29</sup>	1.26	4.60	0.978	0.39(2)	0.90(4)

<sup>a</sup>The interfacial free energy,  $\langle\gamma_{iw}\rangle$ , is given in mJ/m<sup>2</sup>, the melting enthalpy,  $\Delta H_m$ , in kcal/mol, and the melting entropy,  $\Delta S_m$ , in cal/(mol K).

$$\frac{\gamma\rho^{-2/3}}{k_B T_m} = c_L \quad (5)$$

where  $c_L$  is a constant. This relation was found to work better than Turnbull's for the water models studied in ref 21 (TIP4P, TIP4P-Ew, TIPSP-E). We have checked if these relations hold for the water models studied in this work. The parameters involved in the calculation of  $c_T$  and  $c_L$  and the constants themselves are reported in Table 3. Both relations seem to work well within the accuracy of our calculations, although the  $c_T$  and  $c_L$  constants for the mW seem to be a bit off perhaps because it does not belong to the TIP4P family. We would need to decrease the error bar in  $\gamma_{iw}$  in order to discriminate which relation works better. The fact that both relations work reasonably well suggests that  $\Delta h_m$  and  $T_m$  are correlated. The ratio between the melting enthalpy and the melting temperature is the melting entropy, which we report in Table 3. In fact, the melting entropy is quite similar for all studied models, which explains why both relations work similarly well. Substituting the density of the crystal by either the fluid density or an average fluid–crystal density does not improve the relations above.

## SUMMARY AND CONCLUSIONS

We use the recently proposed mold integration method<sup>25</sup> to compute the ice–water interfacial free energy for different ice Ih crystal orientations (basal, primary prismatic, and secondary prismatic) of some widely used water models: TIP4P, TIP4P/2005, TIP4P/Ice and mW.

The models of the TIP4P family predict a lower interfacial free energy for the basal plane than for the prismatic planes and a very similar one for both prismatic planes. For the mW model, we could not resolve differences in interfacial free energy between different crystal orientations. Our results for the interfacial free energies are summarized in Table 1.

The interfacial free energy averaged over all crystal orientations is consistent with that previously calculated by analyzing simulations of ice seeds in supercooled water with classical nucleation theory.<sup>30,31</sup> This consistency indirectly supports classical nucleation theory as a good framework to understand crystal nucleation.

We also obtain the interfacial free energy of ice Ic for the (111), (110), and (100) planes using the TIP4P/Ice model. We find that ice Ic has the same orientationally averaged interfacial free energy as ice Ih, in agreement with our previous seeding work.<sup>32</sup>

The interfacial free energy grows with the melting temperature and the melting enthalpy of the model, in agreement with Turnbull's<sup>88</sup> and Laird's<sup>89</sup> relations.

## AUTHOR INFORMATION

### Corresponding Author

\*E-mail esa01@quim.ucm.es (E.S.).

## Notes

The authors declare no competing financial interest.

## ACKNOWLEDGMENTS

This work was funded by Grant FIS2013/43209-P of the MEC and by the Marie Curie Career Integration Grant 322326-COSAAC-FP7-PEOPLE-2012-CIG. E. Sanz acknowledges financial support from a Ramon y Cajal Fellowship. J. R. Espinosa acknowledges financial support from the FPI Grant BES-2014-067625. Calculations were carried out in the supercomputer facility Tirant from the Spanish Supercomputing Network (RES) (Project QCM-2015-1-0028) and UCM/Santander 910570.

## REFERENCES

- Woodruff, D. P. *The Solid-Liquid Interface*; Cambridge University Press: Cambridge, 1973.
- Pruppacher, H. R. A new look at homogeneous ice nucleation in supercooled water drops. *J. Atmos. Sci.* **1995**, *52*, 1924–1933.
- Ickes, L.; Welti, A.; Hoose, C.; Lohmann, U. Classical nucleation theory of homogeneous freezing of water: thermodynamic and kinetic parameters. *Phys. Chem. Chem. Phys.* **2015**, *17*, 5514–5537.
- Hagen, D. E.; Anderson, R. J.; Kassner, J. L. Homogeneous condensation-freezing nucleation rate measurements for small water droplets in an expansion cloud chamber. *J. Atmos. Sci.* **1981**, *38*, 1236–1243.
- Hage, W.; Hallbrucker, A.; Mayer, E.; Johari, G. P. Crystallization kinetics of water below 150 K. *J. Chem. Phys.* **1994**, *100*, 2743–2747.
- Huang, J. F.; Bartell, L. S. Kinetics of homogeneous nucleation in the freezing of large clusters. *J. Phys. Chem.* **1995**, *99*, 3924–3931.
- Kramer, B.; Hubner, O.; Vortisch, H.; Woste, L.; Leisner, T.; Schwel, M.; Ruhl, E.; Baumgärtel, H. Homogeneous nucleation rates of supercooled water measured in single levitated microdroplets. *J. Chem. Phys.* **1999**, *111*, 6521–6527.
- Stockel, P.; Weidinger, I. M.; Baumgärtel, H.; Leisner, T. Rates of homogeneous ice nucleation in levitated H<sub>2</sub>O and D<sub>2</sub>O Droplets. *J. Phys. Chem. A* **2005**, *109*, 2540–2546.
- Stan, C. A.; Schneider, G. F.; Shevkoplyas, S. S.; Hashimoto, M.; Ibanescu, M.; Wiley, B. J.; Whitesides, G. M. A microfluidic apparatus for the study of ice nucleation in supercooled water drops. *Lab Chip* **2009**, *9*, 2293–2305.
- Murray, B. J.; Broadley, S. L.; Wilson, T. W.; Bull, S. J.; Wills, R. H.; Christenson, H. K.; Murray, E. J. Kinetics of the homogeneous freezing of water. *Phys. Chem. Chem. Phys.* **2010**, *12*, 10380–10387.
- Manka, A.; Pathak, H.; Tanimura, S.; Wolk, J.; Strey, R.; Wyslouzil, B. E. Freezing water in no mans land. *Phys. Chem. Chem. Phys.* **2012**, *14*, 4505–4516.
- Bhabhe, A.; Pathak, H.; Wyslouzil, B. E. Freezing of heavy water (D<sub>2</sub>O) nanodroplets. *J. Phys. Chem. A* **2013**, *117*, 5472–5482.
- Riechers, B.; Wittbracht, F.; Hutten, A.; Koop, T. The homogeneous ice nucleation rate of water droplets produced in a microfluidic device and the role of temperature uncertainty. *Phys. Chem. Chem. Phys.* **2013**, *15*, 5873–5887.
- Laksmono, H.; et al. Anomalous behavior of the homogeneous ice nucleation rate in “no-man's land”. *J. Phys. Chem. Lett.* **2015**, *6*, 2826–2832.
- Baker, M. B. Cloud microphysics and climate. *Science* **1997**, *276*, 1072–1078.

- (16) Cantrell, W.; Heymsfield, A. Production of ice in tropospheric clouds. *Bull. Am. Meteorol. Soc.* **2005**, *86*, 795–807.
- (17) DeMott, P. J.; Prenni, A. J.; Liu, X.; Kreidenweis, S. M.; Petters, M. D.; Twohy, C. H.; Richardson, M. S.; Eidhammer, T.; Rogers, D. C. Predicting global atmospheric ice nuclei distributions and their impacts on climate. *Proc. Natl. Acad. Sci. U. S. A.* **2010**, *107*, 11217–11222.
- (18) Broughton, J. Q.; Gilmer, G. H. Molecular dynamics investigation of the crystal-fluid interface. VI. Excess surface free energies of crystal-liquid systems. *J. Chem. Phys.* **1986**, *84*, 5759–5768.
- (19) Davidchack, R. L.; Laird, B. B. Direct calculation of the crystal-melt interfacial free energies for continuous potentials: Application to the Lennard-Jones system. *J. Chem. Phys.* **2003**, *118*, 7651–7657.
- (20) Handel, R.; Davidchack, R. L.; Anwar, J.; Brukhno, A. Direct calculation of solid-liquid interfacial free energy for molecular systems: TIP4P Ice-water interface. *Phys. Rev. Lett.* **2008**, *100*, 036104.
- (21) Davidchack, R. L.; Handel, R.; Anwar, J.; Brukhno, A. V. Ice Ih-water interfacial free energy of simple water models with full electrostatic interactions. *J. Chem. Theory Comput.* **2012**, *8*, 2383–2390.
- (22) Hoyt, J. J.; Asta, M.; Karma, A. Method for computing the anisotropy of the solid-liquid interfacial free energy. *Phys. Rev. Lett.* **2001**, *86*, 5530–5533.
- (23) Benet, J.; MacDowell, L. G.; Sanz, E. A study of the ice-water interface using the TIP4P/2005 water model. *Phys. Chem. Chem. Phys.* **2014**, *16*, 22159–22166.
- (24) Limmer, D. T.; Chandler, D. Premelting, fluctuations, and coarse-graining of water-ice interfaces. *J. Chem. Phys.* **2014**, *141*, 18C505.
- (25) Espinosa, J. R.; Vega, C.; Sanz, E. The mold integration method for the calculation of the crystal-fluid interfacial free energy from simulations. *J. Chem. Phys.* **2014**, *141*, 134709.
- (26) Jorgensen, W. L.; Chandrasekhar, J.; Madura, J. D.; Impey, R. W.; Klein, M. L. Comparison of simple potential functions for simulating liquid water. *J. Chem. Phys.* **1983**, *79*, 926–935.
- (27) Abascal, J. L. F.; Vega, C. A general purpose model for the condensed phases of water: TIP4P/2005. *J. Chem. Phys.* **2005**, *123*, 234505.
- (28) Abascal, J. L. F.; Sanz, E.; Fernandez, R. G.; Vega, C. A potential model for the study of ices and amorphous water: TIP4P/Ice. *J. Chem. Phys.* **2005**, *122*, 234511.
- (29) Molinero, E. B. Valeria und Moore Water modeled as an intermediate element between carbon and silicon. *J. Phys. Chem. B* **2009**, *113*, 4008–4016.
- (30) Sanz, E.; Vega, C.; Espinosa, J. R.; Caballero-Bernal, R.; Abascal, J. L. F.; Valeriani, C. Homogeneous ice nucleation at moderate supercooling from molecular simulation. *J. Am. Chem. Soc.* **2013**, *135*, 15008–15017.
- (31) Espinosa, J. R.; Sanz, E.; Valeriani, C.; Vega, C. Homogeneous ice nucleation evaluated for several water models. *J. Chem. Phys.* **2014**, *141*, 18C529.
- (32) Zaragoza, A.; Conde, M. M.; Espinosa, J. R.; Valeriani, C.; Vega, C.; Sanz, E. Competition between ices Ih and Ic in homogeneous water freezing. *J. Chem. Phys.* **2015**, *143*, 134504.
- (33) Reinhardt, A.; Doye, J. P. K. Free energy landscapes for homogeneous nucleation of ice for a monatomic water model. *J. Chem. Phys.* **2012**, *136*, 054501.
- (34) Reinhardt, A.; Doye, J. P. K. Note: Homogeneous TIP4P/2005 ice nucleation at low supercooling. *J. Chem. Phys.* **2013**, *139*, 096102.
- (35) Svishchev, I. M.; Kusalik, P. G. Crystallization of liquid water in a molecular dynamics simulation. *Phys. Rev. Lett.* **1994**, *73*, 975–978.
- (36) Quigley, D.; Rodger, P. M. Metadynamics simulations of ice nucleation and growth. *J. Chem. Phys.* **2008**, *128*, 154518.
- (37) Li, T.; Donadio, D.; Russo, G.; Galli, G. Homogeneous ice nucleation from supercooled water. *Phys. Chem. Chem. Phys.* **2011**, *13*, 19807–19813.
- (38) Buhariwalla, C.; Bowles, R.; Saika-Voivod, I.; Sciortino, F.; Poole, P. Free energy of formation of small ice nuclei near the Widom line in simulations of supercooled water. *Eur. Phys. J. E: Soft Matter Biol. Phys.* **2015**, *38*, 39.
- (39) Geiger, P.; Dellago, C. Neural networks for local structure detection in polymorphic systems. *J. Chem. Phys.* **2013**, *139*, 164105.
- (40) Malkin, T. L.; Murray, B. J.; Brukhno, A. V.; Anwar, J.; Salzmann, C. G. Structure of ice crystallized from supercooled water. *Proc. Natl. Acad. Sci. U. S. A.* **2012**, *109*, 1041–1045.
- (41) Moore, E. B.; Molinero, V. Is it cubic? Ice crystallization from deeply supercooled water. *Phys. Chem. Chem. Phys.* **2011**, *13*, 20008–20016.
- (42) Moore, E. B.; Molinero, V. Structural transformation in supercooled water controls the crystallization rate of ice. *Nature* **2011**, *479*, 506–508.
- (43) Russo, J.; Romano, F.; Tanaka, H. New metastable form of ice and its role in the homogeneous crystallization of water. *Nat. Mater.* **2014**, *13*, 733–739.
- (44) Radhakrishnan, R.; Trout, B. L. Nucleation of hexagonal ice (Ih) in liquid water. *J. Am. Chem. Soc.* **2003**, *125*, 7743–7747.
- (45) Cox, S. J.; Kathmann, S. M.; Slater, B.; Michaelides, A. Molecular simulations of heterogeneous ice nucleation. I. Controlling ice nucleation through surface hydrophilicity. *J. Chem. Phys.* **2015**, *142*, 184704.
- (46) Haji-Akbari, A.; Debenedetti, P. G. Direct calculation of ice homogeneous nucleation rate for a molecular model of water. *Proc. Natl. Acad. Sci. U. S. A.* **2015**, *112*, 10582–10588.
- (47) Gibbs, J. W. On the equilibrium of heterogeneous substances. *Trans. Connect. Acad. Sci.* **1876**, *3*, 108–248.
- (48) Gibbs, J. W. On the equilibrium of heterogeneous substances. *Trans. Connect. Acad. Sci.* **1878**, *16*, 343–524.
- (49) Kelton, K. F. *Crystal Nucleation in Liquids and Glasses*; Academic: Boston, 1991.
- (50) Volmer, M.; Weber, A. Keimbildung in übersättigten Gebilden. *Z. Phys. Chem.* **1926**, *119*, 277.
- (51) Becker, R.; Doring, W. Kinetische behandlung der keimbildung in übersättigten dämpfen. *Ann. Phys.* **1935**, *416*, 719–752.
- (52) Murray, B. J.; Knopf, D. A.; Bertram, A. K. The formation of cubic ice under conditions relevant to Earth's atmosphere. *Nature* **2005**, *434*, 202–205.
- (53) Lisgarten, N. D.; Blackman, M. Cubic form of ice. *Nature* **1956**, *178*, 39–40.
- (54) Shallcross, F. V.; Carpenter, G. B. X-ray diffraction study of the cubic phase of ice. *J. Chem. Phys.* **1957**, *26*, 782–784.
- (55) Dowell, L. G.; Rinfret, A. P. Low-temperature forms of ice as studied by x-ray diffraction. *Nature* **1960**, *188*, 1144–1148.
- (56) Bertie, J. E.; Jacobs, S. M. Far-infrared absorption by ices Ih and Ic at 4.3 K and the powder diffraction pattern of ice Ic. *J. Chem. Phys.* **1977**, *67*, 2445–2448.
- (57) Klotz, S.; Besson, J. M.; Hamel, G.; Nelmes, R. J.; Loveday, J. S.; Marshall, W. G. Metastable ice VII at low temperature and ambient pressure. *Nature* **1999**, *398*, 681–684.
- (58) Klug, D. D.; Handa, Y. P.; Tse, J. S.; Whalley, E. Transformation of Ice VIII to amorphous ice by melting at low temperature. *J. Chem. Phys.* **1989**, *90*, 2390–2392.
- (59) Kuhs, W. F.; Sippel, C.; Falenty, A.; Hansen, T. C. Extent and relevance of stacking disorder in ice Ic. *Proc. Natl. Acad. Sci. U. S. A.* **2012**, *109*, 21259–21264.
- (60) Malkin, T. L.; Murray, B. J.; Salzmann, C. G.; Molinero, V.; Pickering, S. J.; Whale, T. F. Stacking disorder in ice I. *Phys. Chem. Chem. Phys.* **2015**, *17*, 60–76.
- (61) Hess, B.; Kutzner, C.; van der Spoel, D.; Lindahl, E. Algorithms for highly efficient, load-balanced, and scalable molecular simulation. *J. Chem. Theory Comput.* **2008**, *4*, 435–447.
- (62) Parrinello, M.; Rahman, A. Polymorphic transitions in single crystals: A new molecular dynamics method. *J. Appl. Phys.* **1981**, *52*, 7182–7190.
- (63) Bussi, G.; Donadio, D.; Parrinello, M. Canonical sampling through velocity rescaling. *J. Chem. Phys.* **2007**, *126*, 014101.
- (64) Wheeler, D. R.; Newman, J. A less expensive Ewald lattice sum. *Chem. Phys. Lett.* **2002**, *366*, 537–543.

- (65) Angioletti-Uberti, S.; Ceriotti, M.; Lee, P. D.; Finnis, M. W. Solid-liquid interface free energy through metadynamics simulations. *Phys. Rev. B: Condens. Matter Mater. Phys.* **2010**, *81*, 125416.
- (66) Fernandez, L. A.; Martin-Mayor, V.; Seoane, B.; Verrocchio, P. Equilibrium fluid-solid coexistence of hard spheres. *Phys. Rev. Lett.* **2012**, *108*, 165701.
- (67) Zykova-Timan, T.; Ceresoli, D.; Tartaglino, U.; Tosatti, E. Why are alkali halide surfaces not wetted by their own melt? *Phys. Rev. Lett.* **2005**, *94*, 176105.
- (68) Zykova-Timan, T.; Ceresoli, D.; Tartaglino, U.; Tosatti, E. Physics of solid and liquid alkali halide surfaces near the melting point. *J. Chem. Phys.* **2005**, *123*, 164701.
- (69) Benjamin, R.; Horbach, J. Crystal-liquid interfacial free energy via thermodynamic integration. *J. Chem. Phys.* **2014**, *141*, 044715.
- (70) Schmitz, F.; Virnau, P. The ensemble switch method for computing interfacial tensions. *J. Chem. Phys.* **2015**, *142*, 144108.
- (71) Espinosa, J. R.; Vega, C.; Valeriani, C.; Sanz, E. The crystal-fluid interfacial free energy and nucleation rate of NaCl from different simulation methods. *J. Chem. Phys.* **2015**, *142*, 194709.
- (72) Lechner, W.; Dellago, C. Accurate determination of crystal structures based on averaged local bond order parameters. *J. Chem. Phys.* **2008**, *129*, 114707.
- (73) Espinosa, J. R.; Vega, C.; Valeriani, C.; Sanz, E. Seeding approach to crystal nucleation. *J. Chem. Phys.* **2016**, *144*, 034501.
- (74) Limmer, D. T.; Chandler, D. Phase diagram of supercooled water confined to hydrophilic nanopores. *J. Chem. Phys.* **2012**, *137*, 044509.
- (75) Seo, M.; Jang, E.; Kim, K.; Choi, S.; Kim, J. S. Understanding anisotropic growth behavior of hexagonal ice on a molecular scale: A molecular dynamics simulation study. *J. Chem. Phys.* **2012**, *137*, 154503.
- (76) Kara, M.; Kurki-Suonio, K. Symmetrized multipole analysis of orientational distributions. *Acta Crystallogr., Sect. A: Cryst. Phys., Diffraction, Theor. Gen. Crystallogr.* **1981**, *37*, 201–210.
- (77) Bai, X.-M.; Li, M. Calculation of solid-liquid interfacial free energy: A classical nucleation theory based approach. *J. Chem. Phys.* **2006**, *124*, 124707.
- (78) Pereyra, R. G.; Szeleifer, I.; Carignano, M. A. Temperature dependence of ice critical nucleus size. *J. Chem. Phys.* **2011**, *135*, 034508.
- (79) Knott, B. C.; Molinero, V.; Doherty, M. F.; Peters, B. Homogeneous nucleation of methane hydrates: Unrealistic under realistic conditions. *J. Am. Chem. Soc.* **2012**, *134*, 19544–19547.
- (80) Rozmanov, D.; Kusalik, P. G. Temperature dependence of crystal growth of hexagonal ice (Ih). *Phys. Chem. Chem. Phys.* **2011**, *13*, 15501–15511.
- (81) Carignano, M. A. Formation of stacking faults during ice growth on hexagonal and cubic substrates. *J. Phys. Chem. C* **2007**, *111*, 501–504.
- (82) Fehner, W. R.; Vosko, S. H. A product representation for cubic harmonics and special directions for the determination of the Fermi surface and related properties. *Can. J. Phys.* **1976**, *54*, 2159–2169.
- (83) Benet, J.; MacDowell, L. G.; Sanz, E. Interfacial free energy of the NaCl crystal-melt interface from capillary wave fluctuations. *J. Chem. Phys.* **2015**, *142*, 134706.
- (84) Garcia-Fernandez, R.; Abascal, J. L. F.; Vega, C. The melting point of ice Ih for common water models calculated from direct coexistence of the solid-liquid interface. *J. Chem. Phys.* **2006**, *124*, 144506.
- (85) Conde, M. M.; Gonzalez, M. A.; Abascal, J. L. F.; Vega, C. Determining the phase diagram of water from direct coexistence simulations: The phase diagram of the TIP4P/2005 model revisited. *J. Chem. Phys.* **2013**, *139*, 154505.
- (86) Weiss, V. C.; Rullich, M.; Köhler, C.; Frauenheim, T. Kinetic aspects of the thermostatted growth of ice from supercooled water in simulations. *J. Chem. Phys.* **2011**, *135*, 034701.
- (87) Yan, J. Y.; Patey, G. N. Molecular dynamics simulations of ice nucleation by electric fields. *J. Phys. Chem. A* **2012**, *116*, 7057–7064.
- (88) Turnbull, D. Formation of crystal nuclei in liquid metals. *J. Appl. Phys.* **1950**, *21*, 1022–1028.
- (89) Laird, B. B. The solid-liquid interfacial free energy of close-packed metals: hard-spheres and the Turnbull coefficient. *J. Chem. Phys.* **2001**, *115*, 2887–2888.